

**Cell Systems, Volume 10**

**Supplemental Information**

**Cellular Dialogues: Cell-Cell Communication  
through Diffusible Molecules Yields  
Dynamic Spatial Patterns**

**Yiteng Dang, Douwe A.J. Grundel, and Hyun Youk**

SUPPLEMENTAL FIGURES

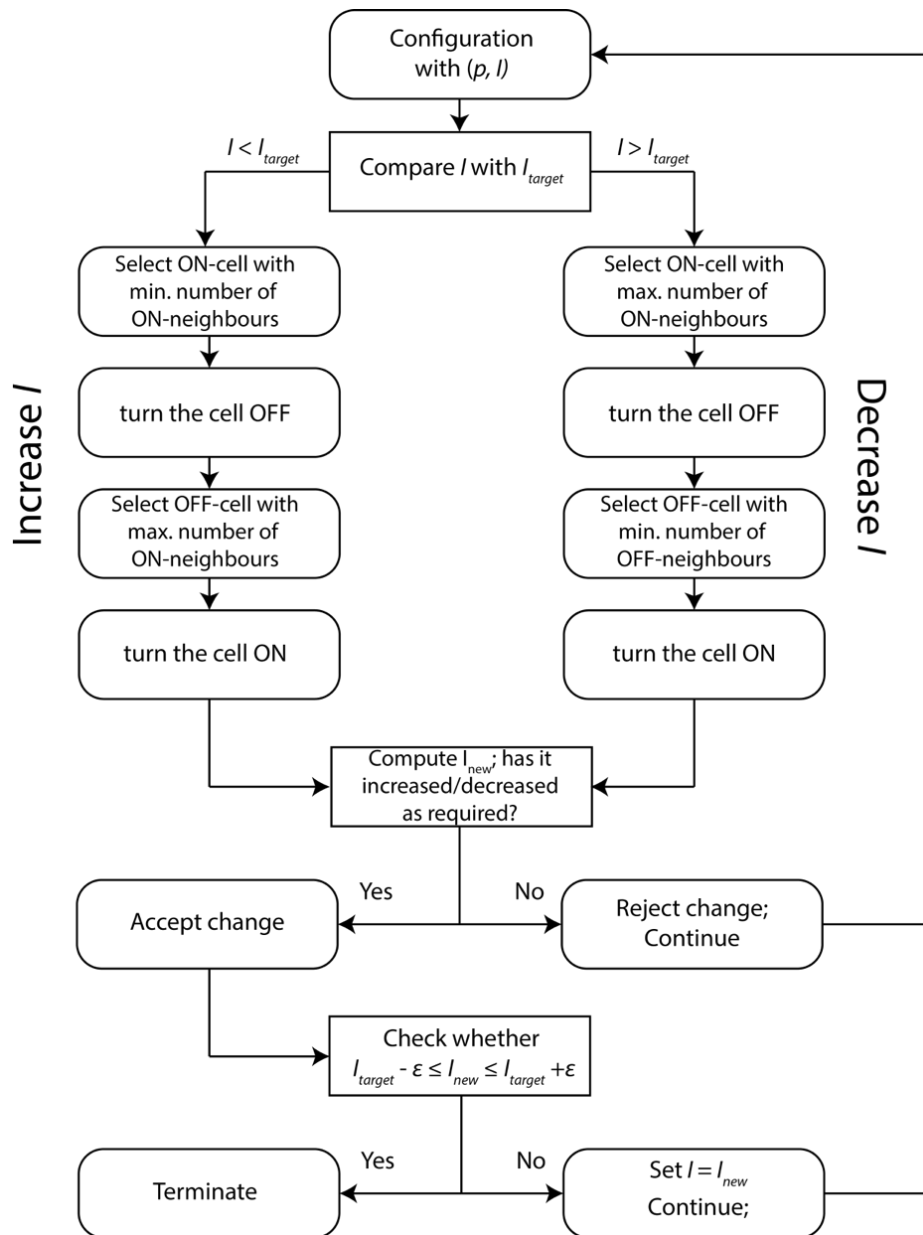


**Figure S1. Algorithm used to generate spatial configurations with a desired value of spatial index  $I^{(i)}$  and a fraction of cells which are ON for gene- $i$  (denoted  $p^{(i)}$ ).**

**(Related to Figure 1)**

STAR Methods defines the two "macrostate" variables,  $I^{(i)}$  (spatial index for gene- $i$ ) and  $p^{(i)}$  (fraction of cells that express gene- $i$  (i.e., ON for gene- $i$ )). Since each cell has two genes - one for each secreted molecule - there are two spatial indices and two  $p$ 's. Atypical simulation, unless stated otherwise, started with a maximally disordered field of cells (i.e., cells' gene-expression levels

were spatially uncorrelated, for both genes). This means that, at the beginning of a simulation, the spatial index  $I^{(i)}$  was zero for both genes. While keeping the spatial indices to be zero, we could set  $p^{(1)}$  and  $p^{(2)}$  to be virtually any value that we desired, by using the algorithm shown here. In short, the algorithm starts with a spatial configuration described by some pair of macroscopic variables  $(p^{(i)}, I^{(i)})$ , which may not have the values that we want. The algorithm then iteratively updates the value of  $I^{(i)}$  while keeping  $p^{(i)}$  constant. It does so by randomly selecting cells and changing their states until we obtain the  $(p^{(i)}, I^{(i)})$  that we want to begin our simulation with. As  $(p^{(i)}, I^{(i)})$  is specific for a single gene (i.e., gene- $i$ ), we can vary  $(p^{(1)}, I^{(1)})$  independently of  $(p^{(2)}, I^{(2)})$ .

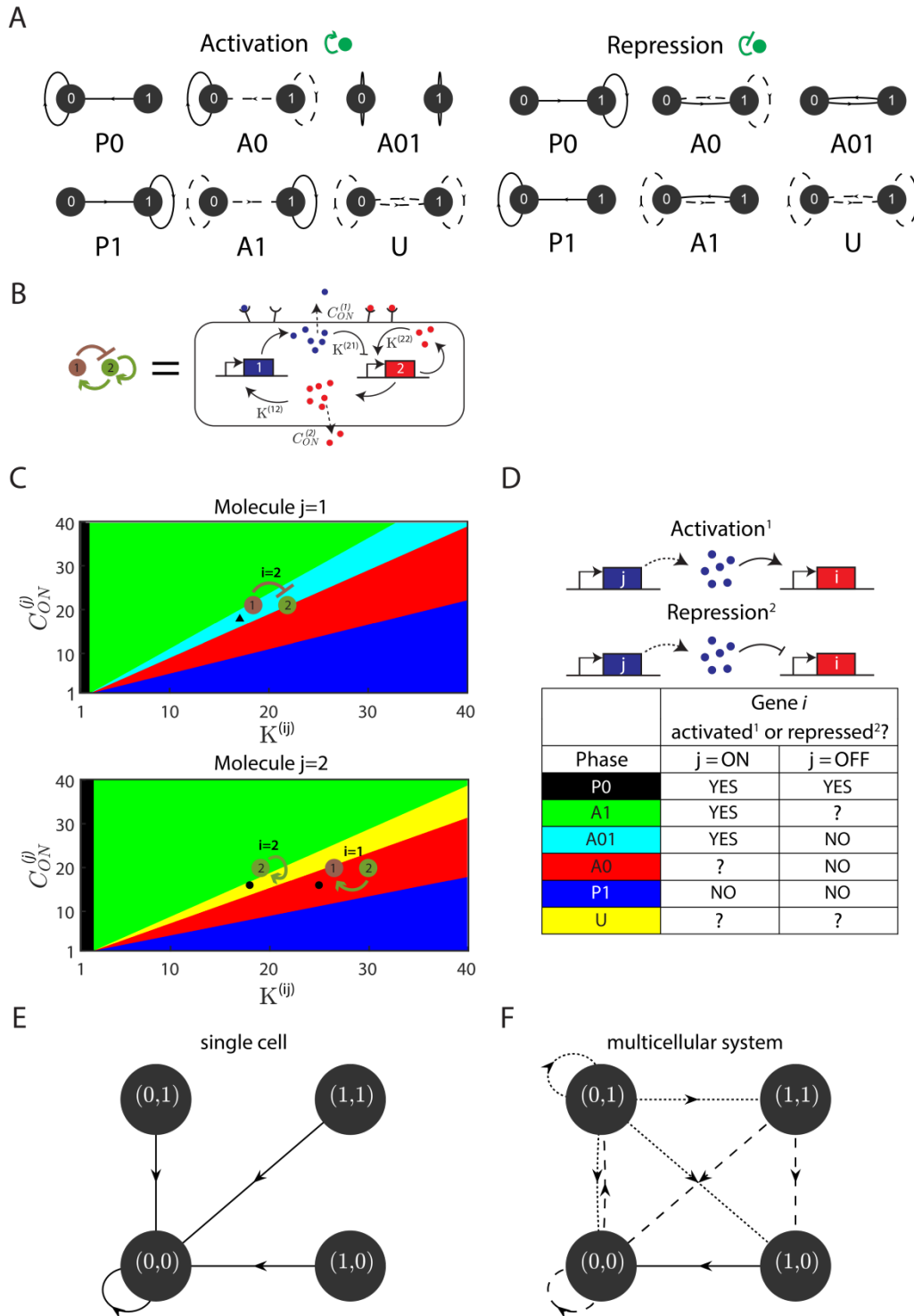


**Figure S2.** Directed graph (state diagram) representation of reveals all the ways in which a cell's gene expression can change and, in turn, what kinds of patterns can form at the population level (also see Supplemental Analysis Section S2).

*(Related to Figure 3)*

Supplemental Analysis Section S2 describes in detail how we obtain a directed graph (state diagram) representation for every cellular dialogue. A directed graph representation allows us to determine which cellular dialogue and for which sets of parameter values a periodic steady-state (dynamic patterns) and/or stationary steady-state (static spatial-configurations) can form without having to run any simulations. **(A)** Overview of all state diagrams for one signaling molecule, corresponding to the six different dynamic phases (Supplemental Analysis Section S2.1) for self-activation (left) and self-inhibition (right). **(B)** Schematic of a cellular dialogue with two signaling molecules. **(C)** A phase diagram - we introduced this in Maire and Youk (*Cell Systems* 2015) and Olimpio et al. (*iScience* 2018) and describe it in Supplemental Analysis Section S2 - shows the phase (colored region) associated with each regulatory interaction of a cellular dialogue as function of the threshold concentration  $K^{(ij)}$  and maximal secretion rate  $C_{ON}^{(j)}$  for every regulatory interaction  $i \leftarrow j$ . **(D)** Each phase imposes different constraints on each regulatory interaction of a cellular dialogue. The regulated gene may be activated (or repressed), or the outcome is unknown and depends on other elements (indicated by "?"). **(E-F)** Considering the constraints imposed by the phase diagrams, we constructed state diagrams that summarize all possible temporal changes that a cell's gene-expression can have. Solid lines indicate deterministic transitions, whereas dashed lines indicate that a cell can have multiple possible transitions to a different gene-expression state. **(E)** A state diagram for a population of one cell. **(F)** State diagram for a population of multiple cells.

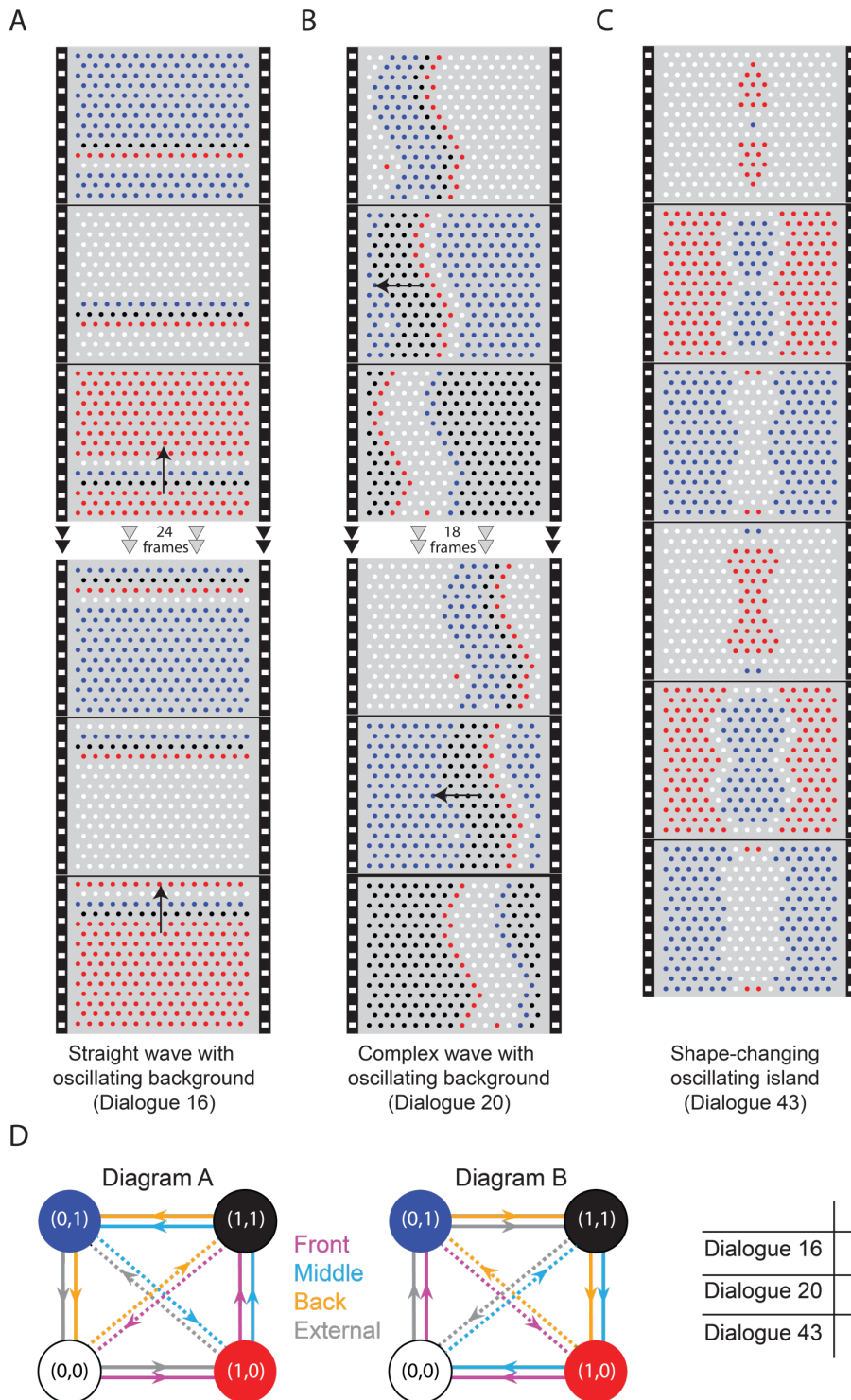


**Figure S3. Dynamic patterns with oscillating cells in their background and their associated state diagrams.**

**(Related to Figure 3)**

**(A-C)** Examples of dynamic spatial patterns with oscillating cells (in blue) in their background, generated by cellular dialogues 16, 20, and 43 (see Figure 3D). Time progresses vertically downwards, with subsequent frames separated by one timestep unless indicated otherwise. **(D)** State diagrams showing all possible ways that a cell's gene-expression can change over time, for cellular dialogues 16, 20, and 43 shown in (A-C) (see Supplemental Analysis Section S2). Every cell shown in the filmstrips of (A-C) cycle through three different states before the pattern moves to the next row of cells. The transitions between these single-cell states (nodes in the graphs) are depicted in the state diagrams as directed cycles of a graph. Different colors indicate different relative positions of the cells (matching the colors in Figure 4A). One of these transitions - indicated by the dashed lines - is concurrent with the displacement of the pattern. There are two possible state diagrams for the three cellular dialogues that generate oscillatory dynamic spatial-patterns, as indicated in this table.

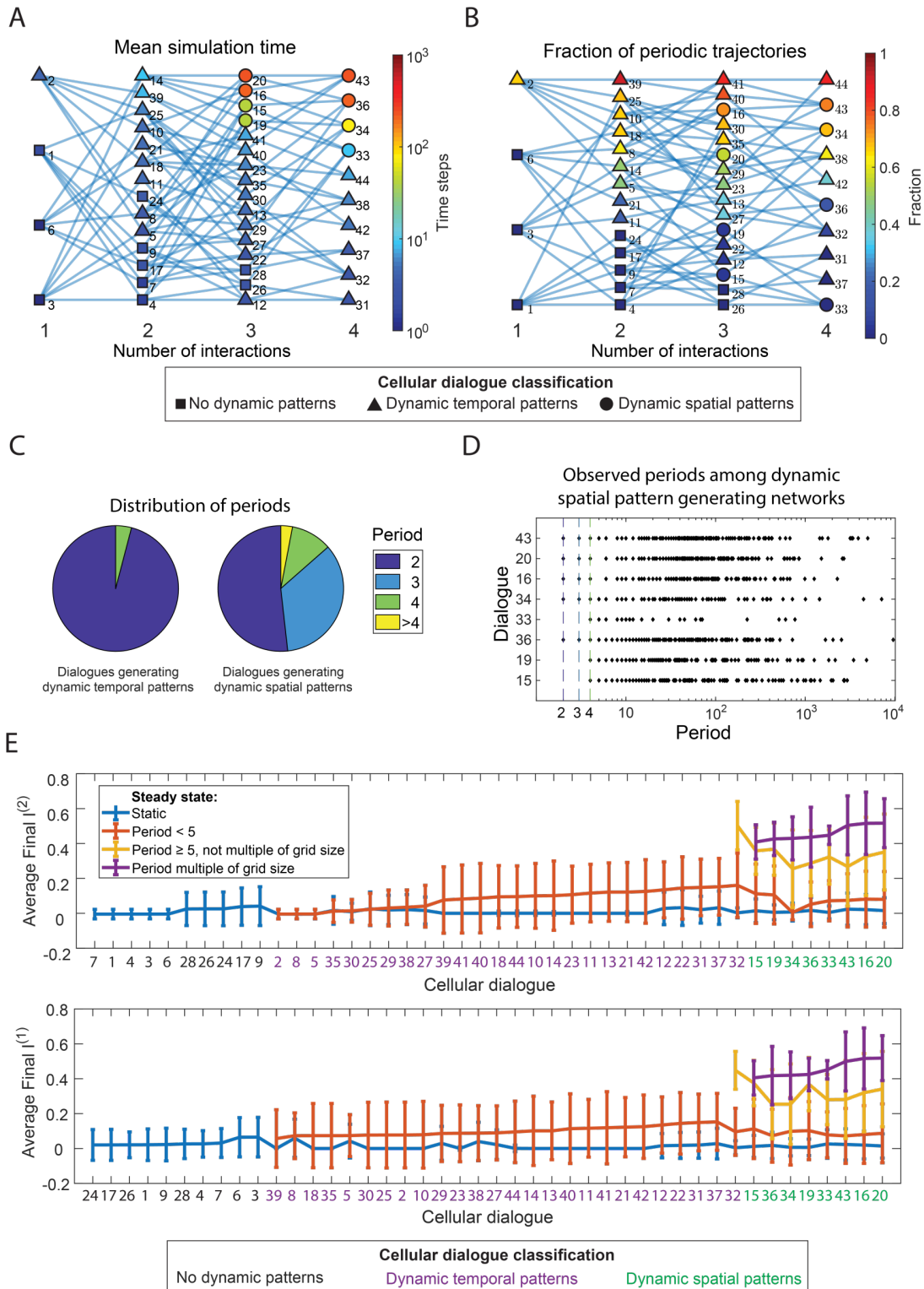
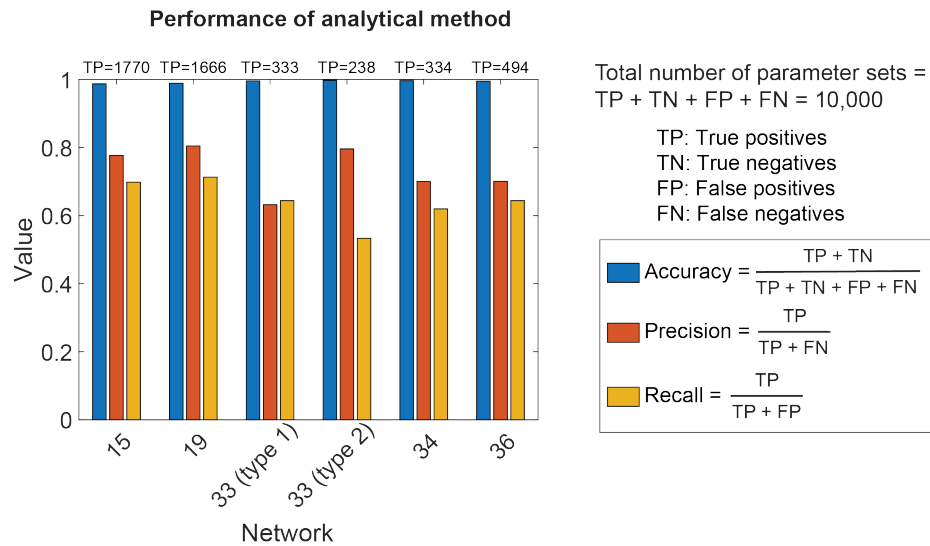


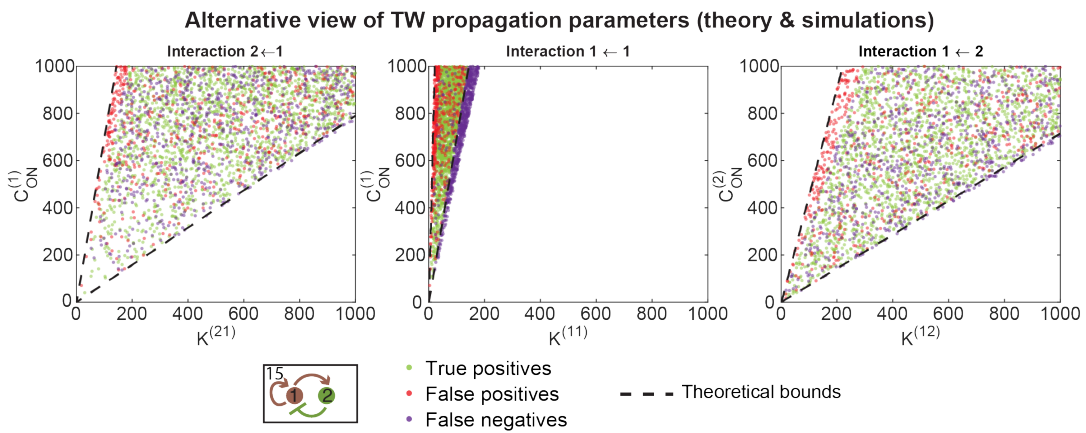
**Figure S4. Statistics for each of the three classes of cellular dialogues in Figures 3B-D. (Related to Figure 3)**

All results are based on the same simulation data set also used to generate Figure 3E, obtained from Latin hypercube sampling over various system parameters (see STAR Methods). **(A)** Mean simulation time across all simulations of a given network. The simulation time is the time it takes for the system to reach equilibrium or the maximum simulation time if a trajectory never reaches equilibrium. Same graphical representation as in Figure 3E. **(B)** Fraction of trajectories with a periodic final state, i.e. a steady state where the final pattern repeats itself after a fixed number of time steps greater than one. Same graphical representation as in Figure 3E. **(C)** Distribution of the periods of the periodic final states among networks that generate dynamic temporal patterns (Figure 3C) and networks that also generate dynamic spatial patterns (Figure 3D). **(D)** Trajectory periods found in simulations of the networks generating dynamic spatial patterns (Figure 3D). Each diamond represents a period that was observed in at least one simulation. **(E)** Average final spatial index for each of the two genes, sorted by cellular dialogue. The trajectories are divided into different classes depending on the final period of the trajectory (represented by differently colored lines). The average is taken over all trajectories within each class. For example, the purple data points show the average values for the subset of trajectories that have a period which is a multiple of the grid size. Error bars represent s.e.m.

A



B



C

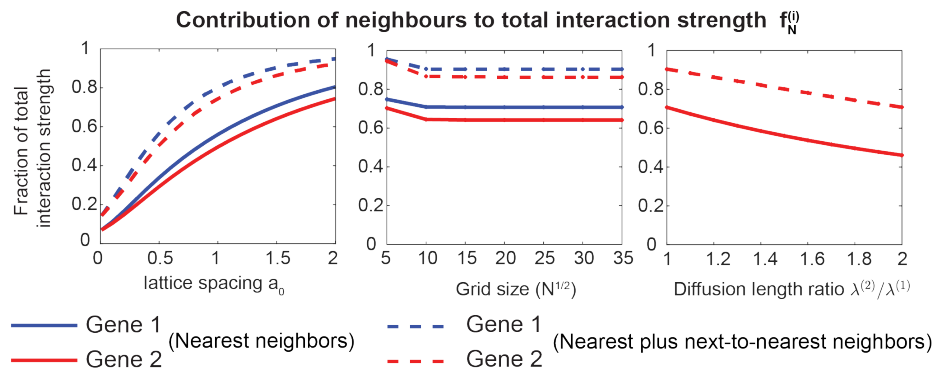
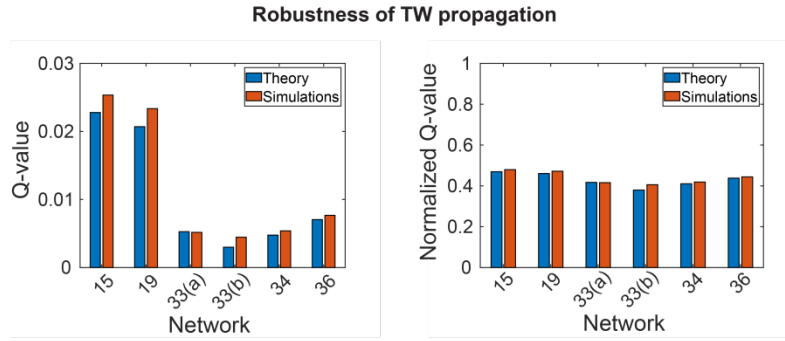


**Figure S5 Comparing simulations with analytical theory for understanding when waves propagate (also see Supplemental Analysis Section S3.5).**

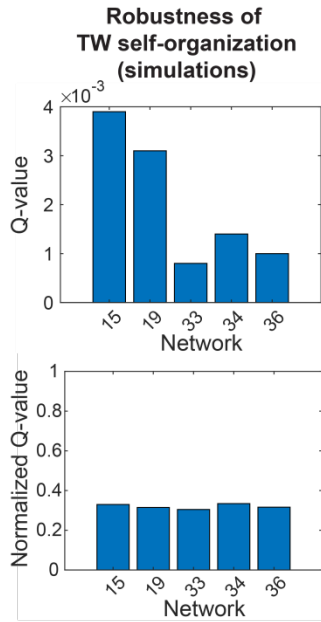
**(Related to Figure 4)**

**(A)** We used concepts from machine learning to quantify the performance of our analytical theory. Specifically, when viewed as a binary classifier, the analytic theory makes binary (yes or no) predictions about whether a parameter set is capable of propagating traveling waves. We compare these predictions with actual simulations to determine whether they are correct or false. The performance of the theory can then be quantified in terms of concepts such as accuracy, precision and recall (see Supplemental Analysis Section S3.5). **(B)** Two-dimensional projections of the parameter sets that are capable of propagating traveling waves according to the analytical theory and exact simulations (see Figure 4F for alternate representations in terms of radar charts). Since there are six varying parameters for each parameter set, we projected the parameter sets onto two-dimensional spaces spanned by the two parameters describing the strength of each interaction – the threshold  $K^{(ij)}$  and the maximum secretion rate  $C_{ON}^{(j)}$ . We plot the data points classified as true positives, false positives and false negatives (see Supplemental Analysis Section S3.5), but leave out the true negatives, which are the parameter sets which are correctly predicted to be incapable of sustaining traveling waves. **(C)** Contribution of nearest-neighbors ( $f_{nn}$ ) and next-to-nearest neighbors ( $f_{nnn}$ ) to the total interaction strength (see Supplemental Analysis Section S3.3.4), as a function of the lattice spacing, the grid size and the ratio between the diffusion lengths. We plot the contribution from nearest neighbors and next-to-nearest neighbors as a fraction of the total interaction strength.

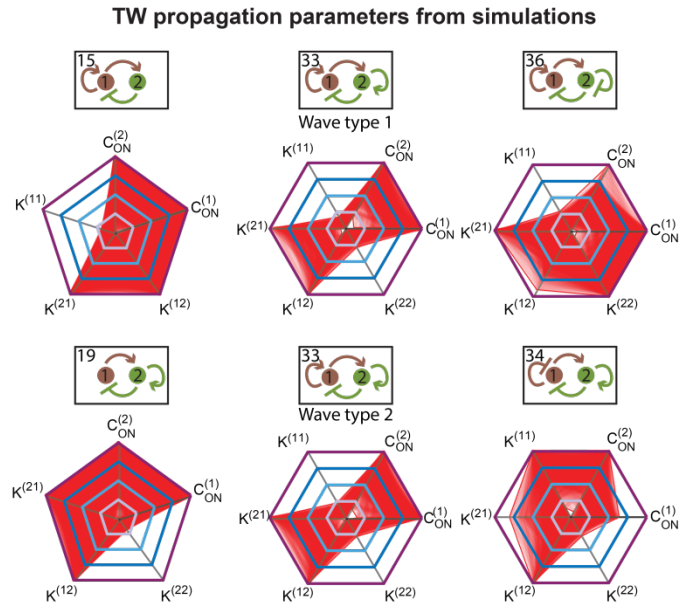
A



B



C



D

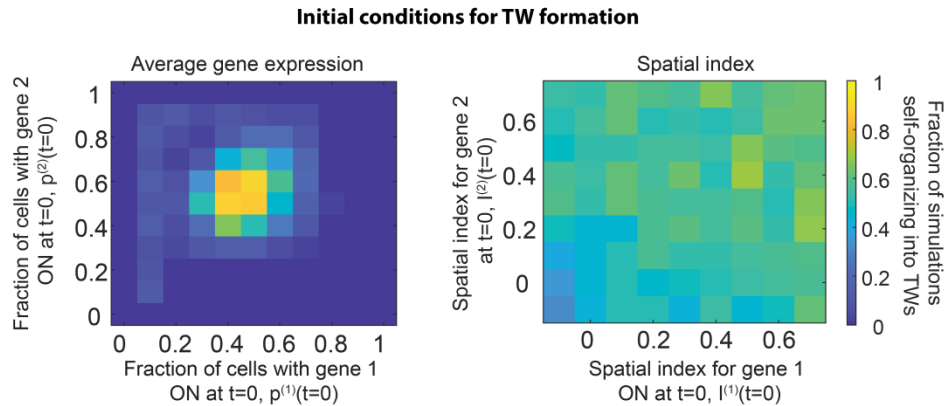


**Figure S6. Robustness of Traveling Waves (TWs), which measures whether large variations in parameter values still yield waves (also see Supplemental Analysis Section S4).**

*(Related to Figures 4 and 5)*

**(A)** We defined robustness as the fraction of parameter sets that were capable of propagating a TW ("Q-value" - see Supplemental Analysis Section S4.1). Here we show the robustness of TW propagation for each cellular dialogue that is capable of generating TWs. Networks 33(a) and 33(b) refer to the two types of TWs that cellular dialogue 33 can generate (see Figure 4D). The normalized Q-value considers the number of parameters for each parameter set and can be interpreted as the probability that a single random draw of each parameter value yields a TW (See Supplemental Section S4.1). Results are based on testing  $10^6$  randomly generated parameter sets obtained from Latin hypercube sampling for both theory and simulations (see STAR Methods). **(B)** Robustness of TW self-organization from random initial states. Results are based on testing  $10^4$  parameter sets, with 10 simulations for each parameter set. **(C)** Radar charts or spider charts for the parameter sets for which TWs propagate as found in simulations (compare with theoretical results in Figure 4F). **(D)** Case studies of the influence of initial state on TW formation. We varied the initial  $p^{(i)}$  – fraction of cells with gene  $i$  ON – for cellular dialogue 15 at fixed parameter values (left plot) and the initial spatial index  $l^{(i)}$  for each of the two genes, for cellular dialogue 19 at fixed parameter values (right plot). For each combination of initial values, we performed 100 simulations.

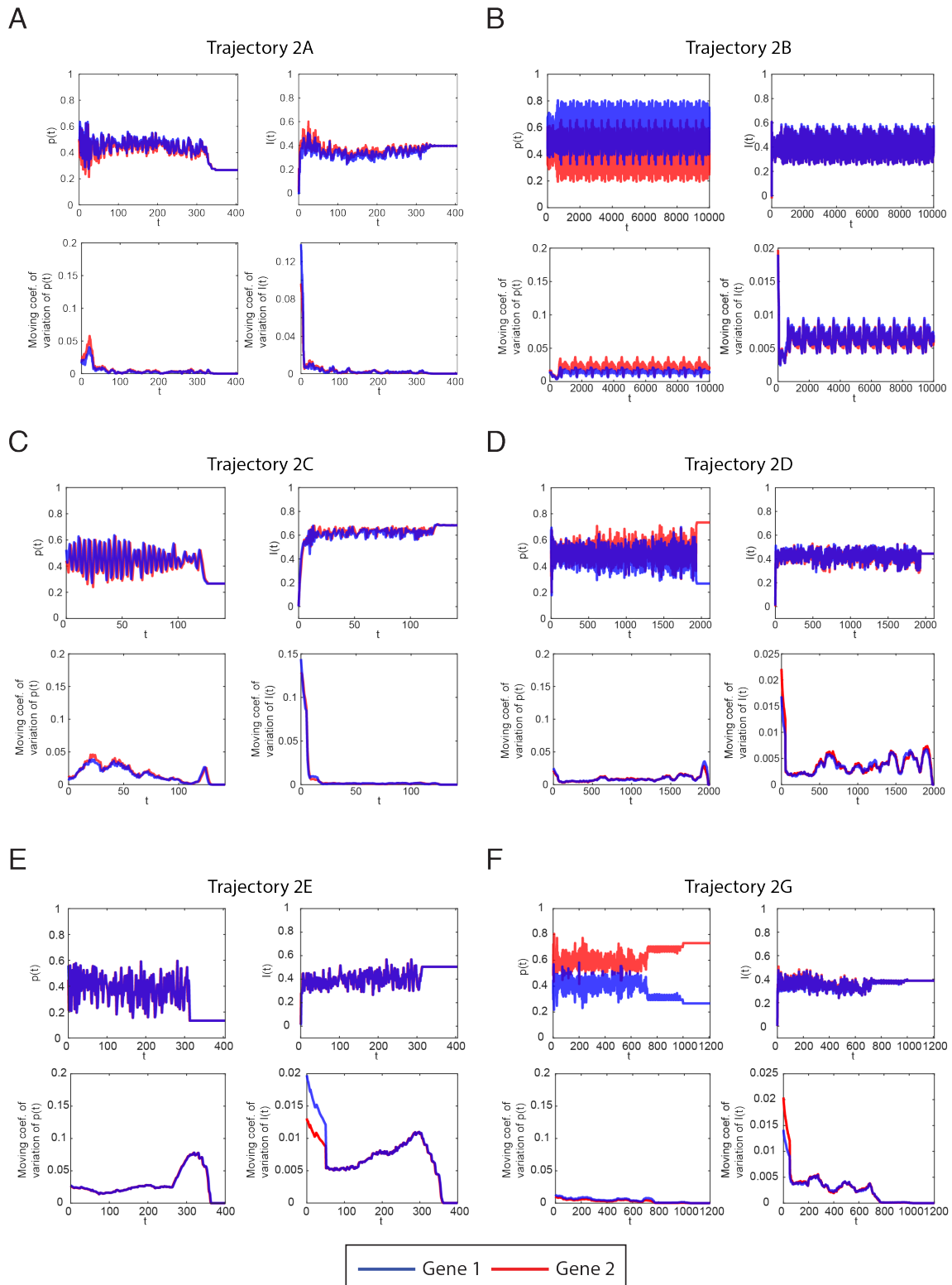
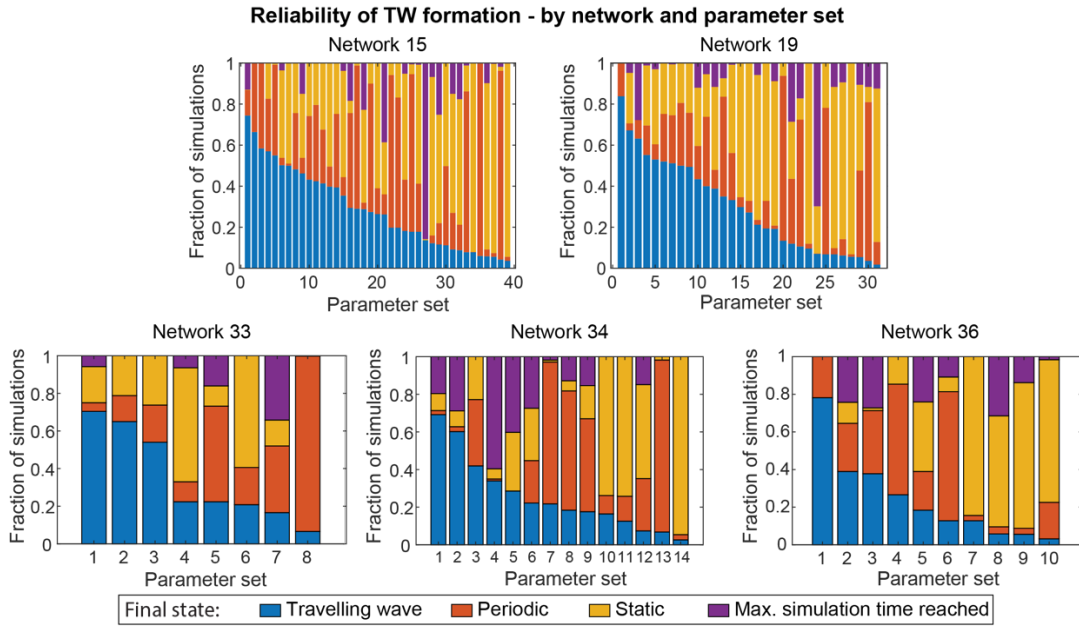


**Figure S7. Additional examples showing how the two macroscopic variables - spatial index and fraction of cells that are ON for gene- $i$  - vary over time during self-organization of dynamic spatial patterns.**

**(Related to Figure 5)**

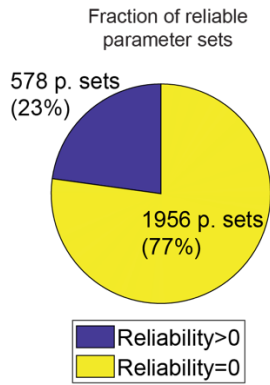
**(A-F)** Plots show how the fraction of cells that have a certain gene ON and the “spatial index” for that gene changes over time (see STAR Methods). Each panel here corresponds to one of the filmstrips shown in Figure 2, as indicated by the panel titles. Time is in units of discrete time steps. Blue curves correspond to gene 1 and red curves correspond to gene 2. For each pattern-forming dynamics, we show four graphs corresponding to the graphs shown in Figures 5B and 5C. Upper left: mean fraction of cells  $p(t)$  that have the indicated gene ON. Lower left: Moving coefficient of variation for  $p(t)$  (see STAR Methods). Upper right: Spatial index  $I(t)$  for the indicated gene. Lower right: Moving coefficient of variation for  $I(t)$  (see STAR Methods).

A

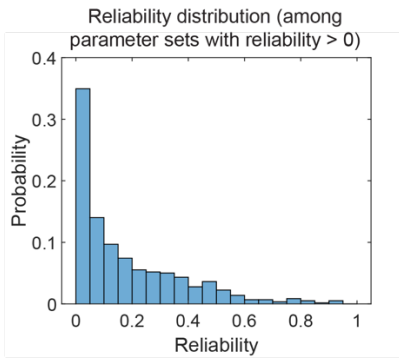


**Reliability of self-organization - parameter sets that can propagate TWs**  
(Network 15,  $n=2534$ )

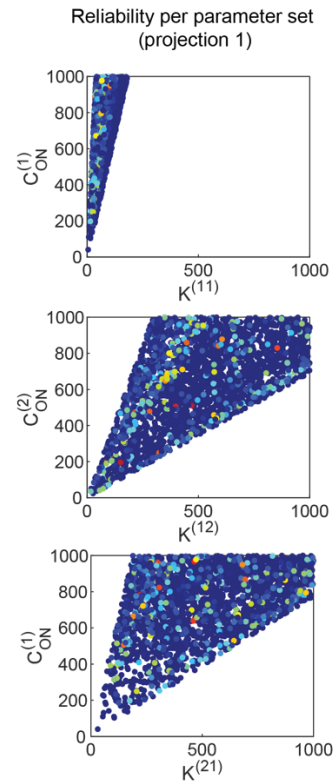
B



C



D



E

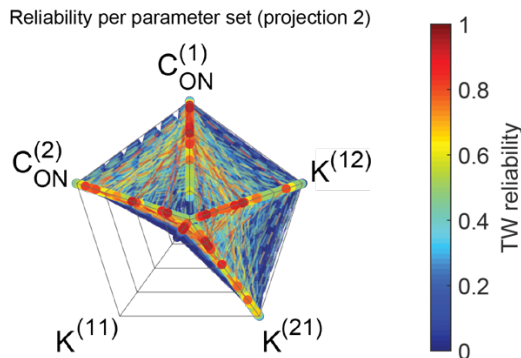


**Figure S8. How reliably Traveling Waves (TWs) can form (also see Supplemental Analysis Section S4.3).**

*(Related to Figure 5).*

We defined "reliability of TW formation" as the fraction of simulations that start with disordered spatial-configurations which then form TWs (see Supplemental Analysis Section S4.3). **(A)** Reliability values for all parameter sets that led to TWs, for each of the five cellular dialogues that can generate dynamic spatial-patterns. The parameter sets are ordered from those that generated the highest number of TWs to those that generated the lowest number of TWs (blue bars). We classified the other simulations as "other periodic patterns" (red), "static patterns" (yellow) and simulations that did not reach either a periodic or a static steady-state (purple). We performed 500 simulations with random initial spatial-configurations for each parameter set. **(B-E)** Reliability of TW *formation* for a large set of parameters ( $n = 2534$ ) capable of *propagating* TWs (i.e., for which a TW initial state continued to propagate indefinitely). For each parameter set, we performed 100 simulations to test whether random initial conditions led to self-organization of TWs. **(B)** Fraction of parameter sets that yielded at least one self-organized TW. **(C)** Distribution of reliability values among the set of parameters with positive values for reliability. **(D-E)** Reliability shows no clear dependence on any of the five parameters that we varied. **(D)** Projection of the five-dimensional parameter sets on the two-dimensional parameter space, spanned by the two parameters that specify the strength of each interaction (see Figure S5B for details). Each dot represents one parameter set and the color represents the reliability (color bar shared with Figure S5B). **(E)** Spider chart projection. Each connected thread represents one parameter set, with the color of the thread representing the reliability for that parameter set.

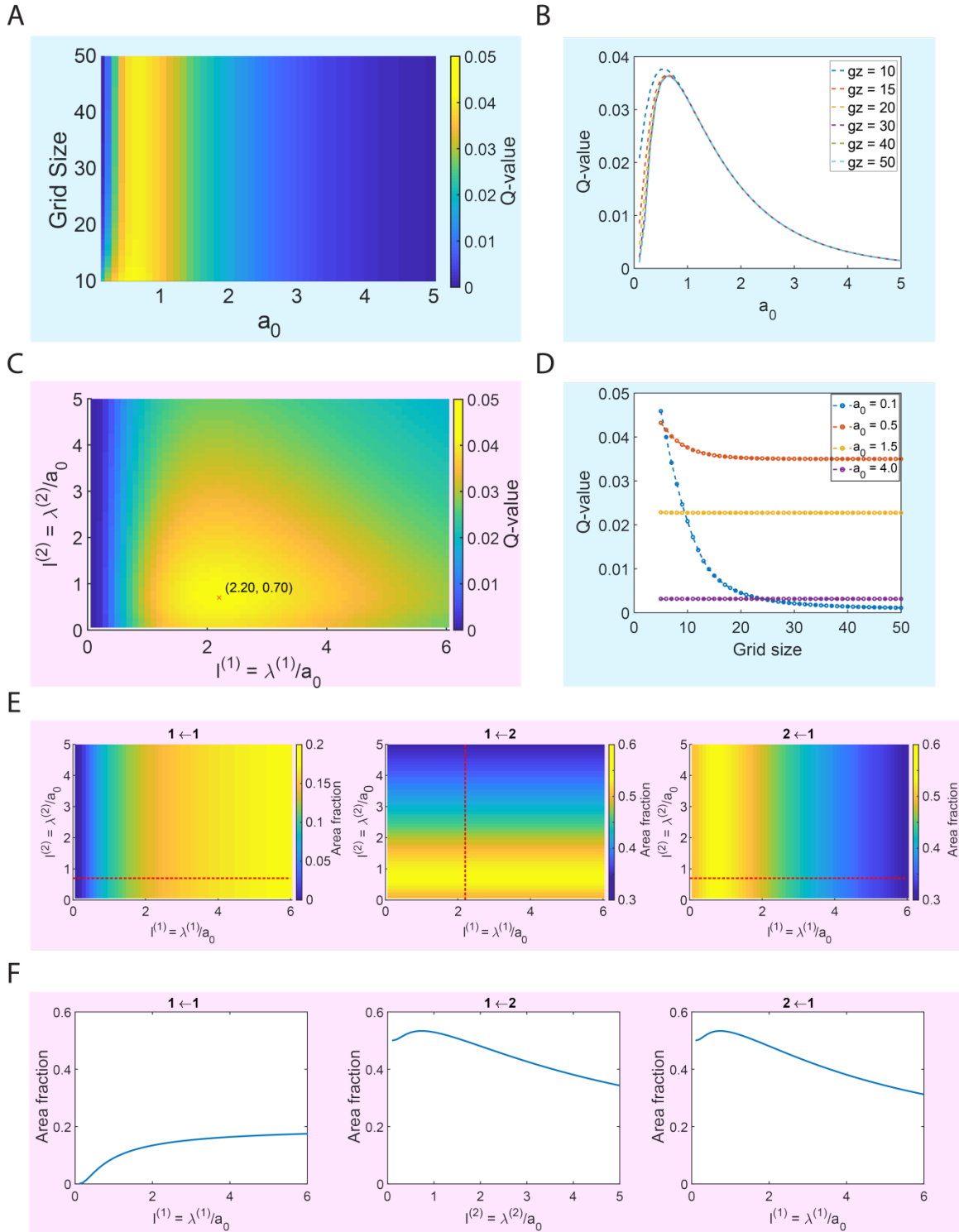


**Figure S9. Analytical framework predicts robustness of wave formations (also see Supplemental Analysis Section S4.2).**

*(Related to Figure 5).*

We used our analytical framework to compute how the robustness –defined as the Q-value (i.e., fraction of parameter sets that enable wave propagation) – varies with the number of cells in a population (light blue plots), nearest-neighbor distance  $a_0$  (i.e., lattice spacing), and diffusion lengths  $l^{(1)}, l^{(2)}$  (see STAR Methods) (pink plots). **(A-D)** Q-value as a function of these parameters. (B) and (D) are one-dimensional sections of the plot in (A), obtained by fixing one of the two parameters while varying the other. **(E-F)** Area fractions are fractions of the two-dimensional parameter space spanned by  $K^{(ij)}, C_{ON}^{(j)}$  for a single interaction  $i \leftarrow j$  that allow for wave propagation (also see Supplemental Analysis Section S4.2). We show here how the area fractions vary with the diffusion lengths  $l^{(1)}, l^{(2)}$ . Red dotted lines in (E) show how we fixed one of these two parameters to obtain the plots in (F).

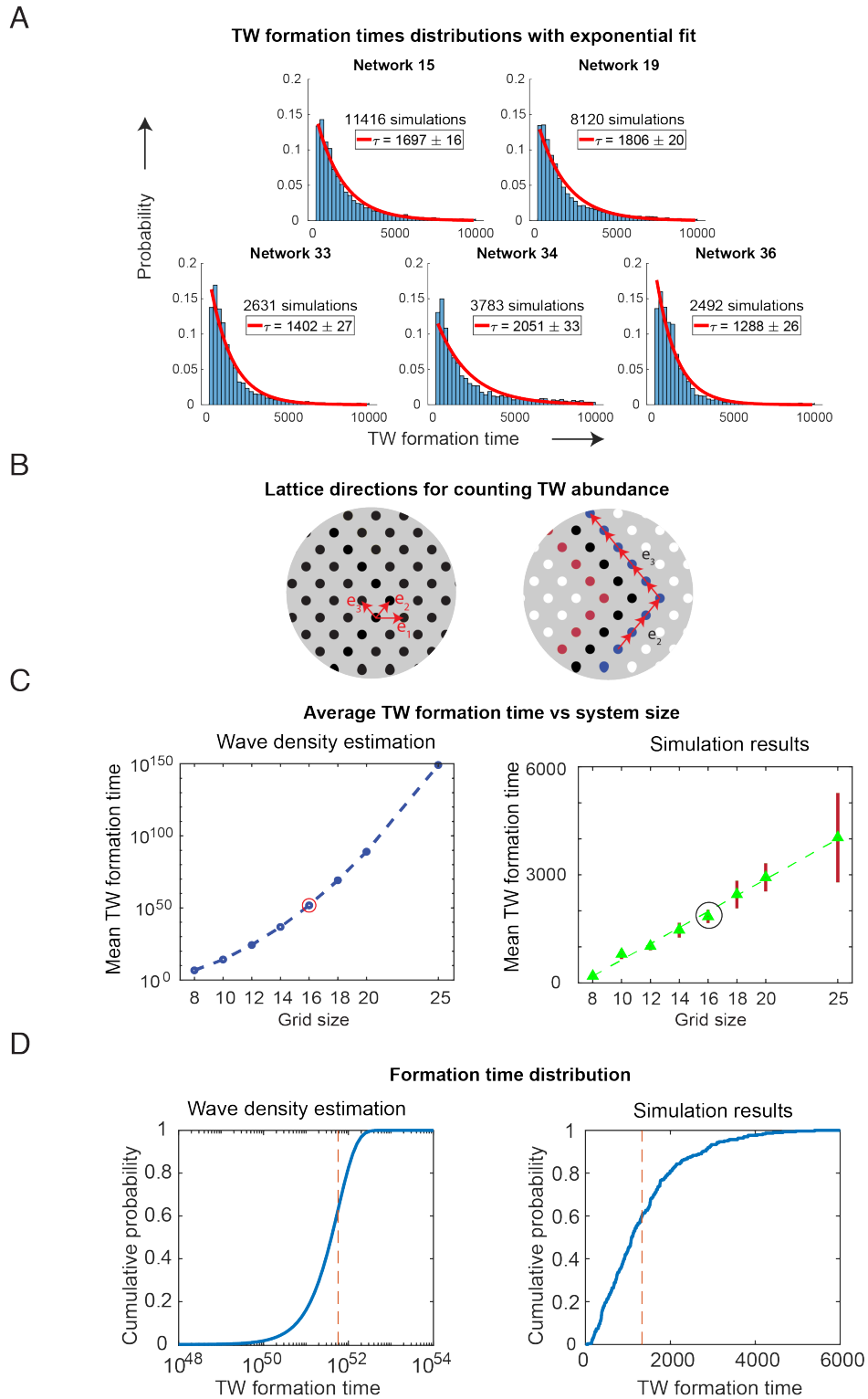


**Figure S10. Statistics on how long cells take to form Traveling Waves (TW). (Related to Figure 5).**

**(A)** TW formation-time distributions from simulations (shown together in Figure 5G) are fitted by exponential functions, with  $\tau$  being the expectation value of the fitted exponential distribution. **(B-D)** Analytic calculation reveals that TW formation times do not follow an entirely random process, i.e. one where each next system state is randomly drawn from the set of all states, as one might suspect based on the chaotic appearance of the dynamics and the exponentially distributed formation times (see Supplemental Analysis Section S3.2). **(B)** Constructions used in the calculation of the abundance of traveling waves in the system (see Supplemental Analysis Section S3.2). (Left) Directions on the lattice. (Right) Sketch of the construction used to characterize a single wave. By counting all ways of traversing the lattice, subject to certain constraints, we obtain an estimate of the number of forms of traveling waves of a given type. **(C)** Average TW formation time estimated from the wave density calculation (left) at different grid sizes, compared with the empirical findings from exact simulations (right). Averages are taken over all self-organized TWs among 300 simulations per grid size, at fixed parameter values. Error bars represent s.e.m. The highlighted data point is the grid size used in (D). **(D)** The cumulative distribution of TW formation times according to the wave density estimation (top) and from simulations (bottom; from simulation set for grid size 16 also used in C). The red dotted line represents the average formation time.

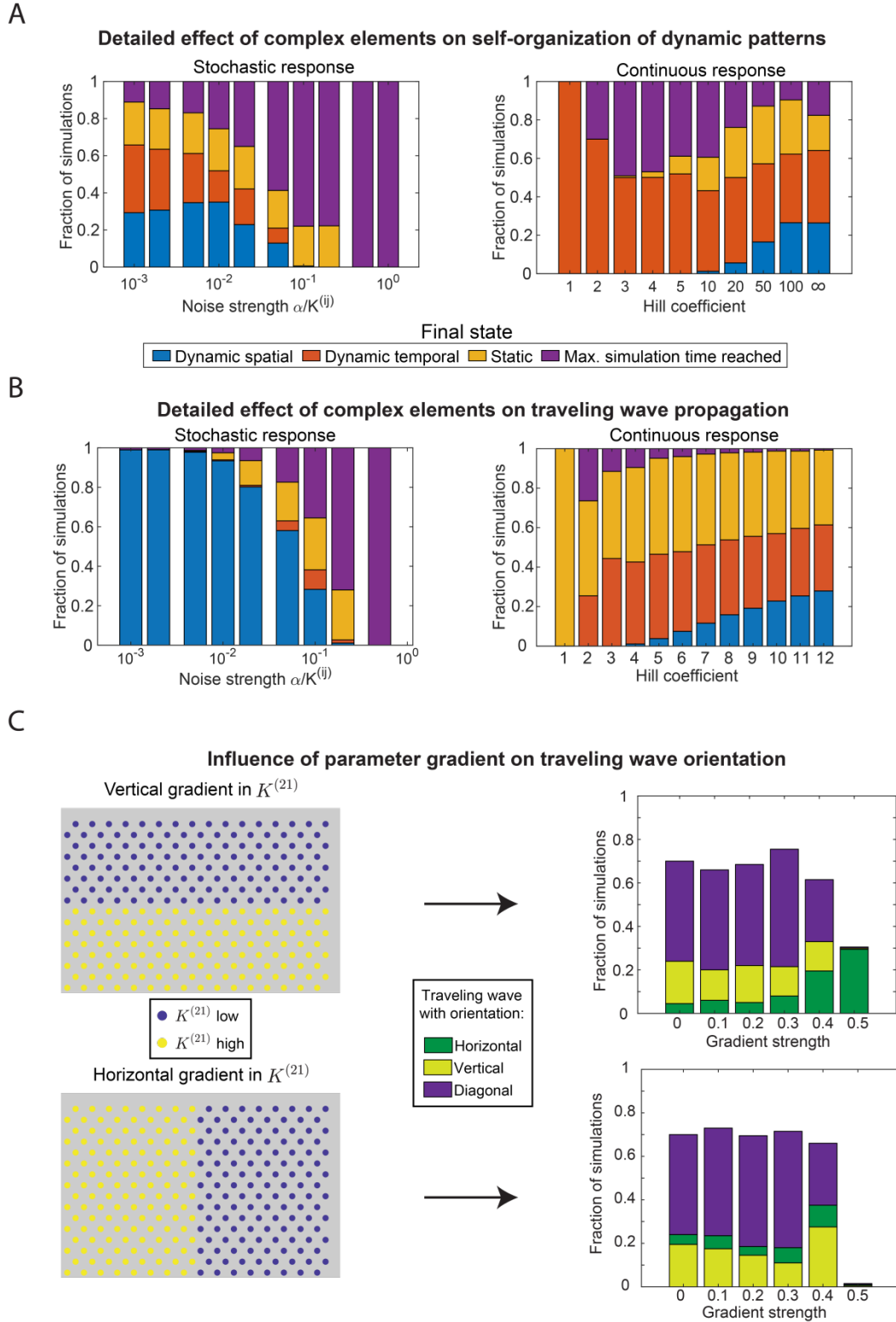


**Figure S11. How noisy gene-expression, finite Hill coefficient, and spatially changing parameter values (as a gradient) influence formation of dynamic patterns and persistence of an already-formed traveling wave.**

**(Related to Figure 6).**

**(A-B)** Detailed breakdown of simulations with two of the complex elements – stochastic response and continuous response – into four classes of patterns. Dynamic spatial pattern here refers to traveling waves specifically, dynamic temporal patterns to all other simulations that yielded periodic steady states, static patterns to simulations where the final state was non-periodic and max. simulation time reached to simulations that never settled down to a steady state within the total simulation time (10,000 timesteps). **(A)** Effect of complex elements on the formation of dynamic patterns, corresponding to the data also used in Figure 6E (upper panels). We performed 200 simulations for each value of the noise and 150 simulations for each value of Hill coefficient. **(B)** Effect of complex elements on traveling wave propagation, corresponding to the data also used in Figure 6D (upper panels). We performed 1,000 simulations for each value of the noise and 2,534 simulations for each value of Hill coefficient. Each simulation corresponds to a different parameter set for which in the absence of noise and with infinite Hill coefficient a straight traveling wave, such as depicted in the lower panel of Figure 6B, can propagate. **(C)** Effect of a parameter gradient on the orientation of formed traveling waves. Specifically, we considered a step-function gradient for the threshold parameter  $K^{(21)}$  oriented along either the vertical direction (upper panels) or horizontal direction (lower panels). We classified the orientation of the formed traveling waves as the relative gradient strength (see STAR Methods) is increased. The unclassified simulations in the bar graphs did not form traveling waves. We performed 200 simulations for each value of the gradient strength.

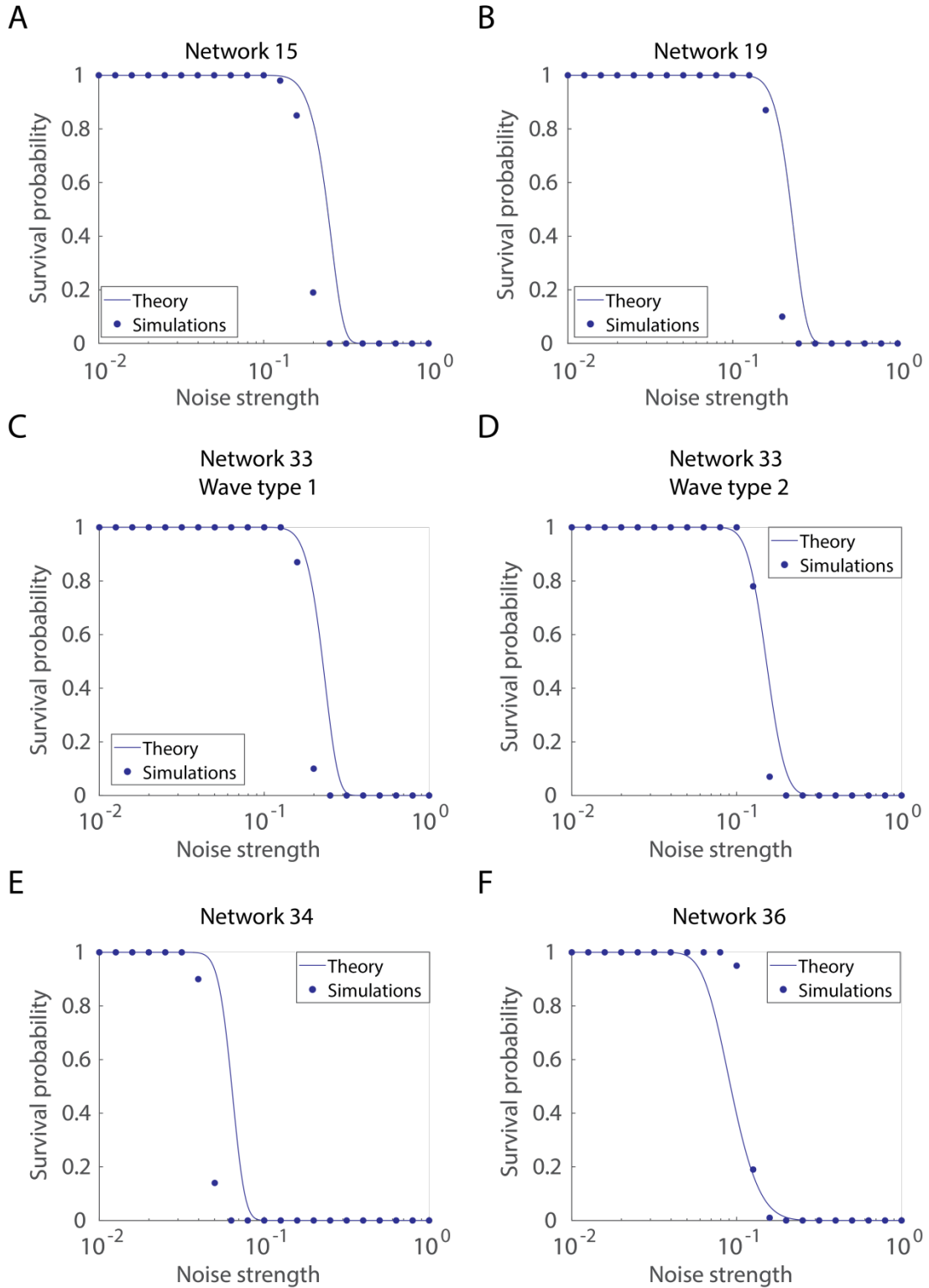


**Figure S12. Persistence of traveling waves in the extended model with stochasticity: theory and simulations (see Supplemental Analysis Section S4.6).**

**(Related to Figure 6)**

**(A-F)** We used the analytical framework for studying wave propagation (Figure 4) to understand how adding noise affects wave propagation. We introduced noise by stochastically varying the threshold concentrations (i.e.,  $K^{(ij)}$ ) and defined "noise strength" that quantifies the typical fluctuations in  $K^{(ij)}$  (see STAR Methods). The plots here show "survival probability" – the probability that a rectilinear wave, after forming, persists (keeps on traveling) for at least one full period – as a function of the noise strength for all six cellular dialogues that we identified as capable of forming dynamic spatial patterns (Figure 4D). Solid curves in the plots are from our analytical framework, which had no fitting parameters. The data points are from simulations, with 100 iterations of simulations performed for each data point. These results are for fixed sets of parameter values which we chose to lie well within the region of the parameter space where one obtains persistent waves (see, for example, Figure S5B for these regions). Specifically, we chose the following parameters:  $N = 225$ ,  $a_0 = 1.5$ ,  $r_{cell} = 0.2$ ,  $C_{ON} = (500 \ 500)$  (fixed for all cases), and **(A)**  $K = \begin{pmatrix} 50 & 300 \\ 300 & 0 \end{pmatrix}$ , **(B)**  $K = \begin{pmatrix} 50 & 500 \\ 300 & 0 \end{pmatrix}$ , **(C)**  $K = \begin{pmatrix} 40 & 500 \\ 300 & 50 \end{pmatrix}$ , **(D)**  $K = \begin{pmatrix} 50 & 500 \\ 300 & 70 \end{pmatrix}$ , **(E)**  $K = \begin{pmatrix} 900 & 300 \\ 400 & 50 \end{pmatrix}$ , **(F)**  $K = \begin{pmatrix} 900 & 400 \\ 300 & 50 \end{pmatrix}$ .

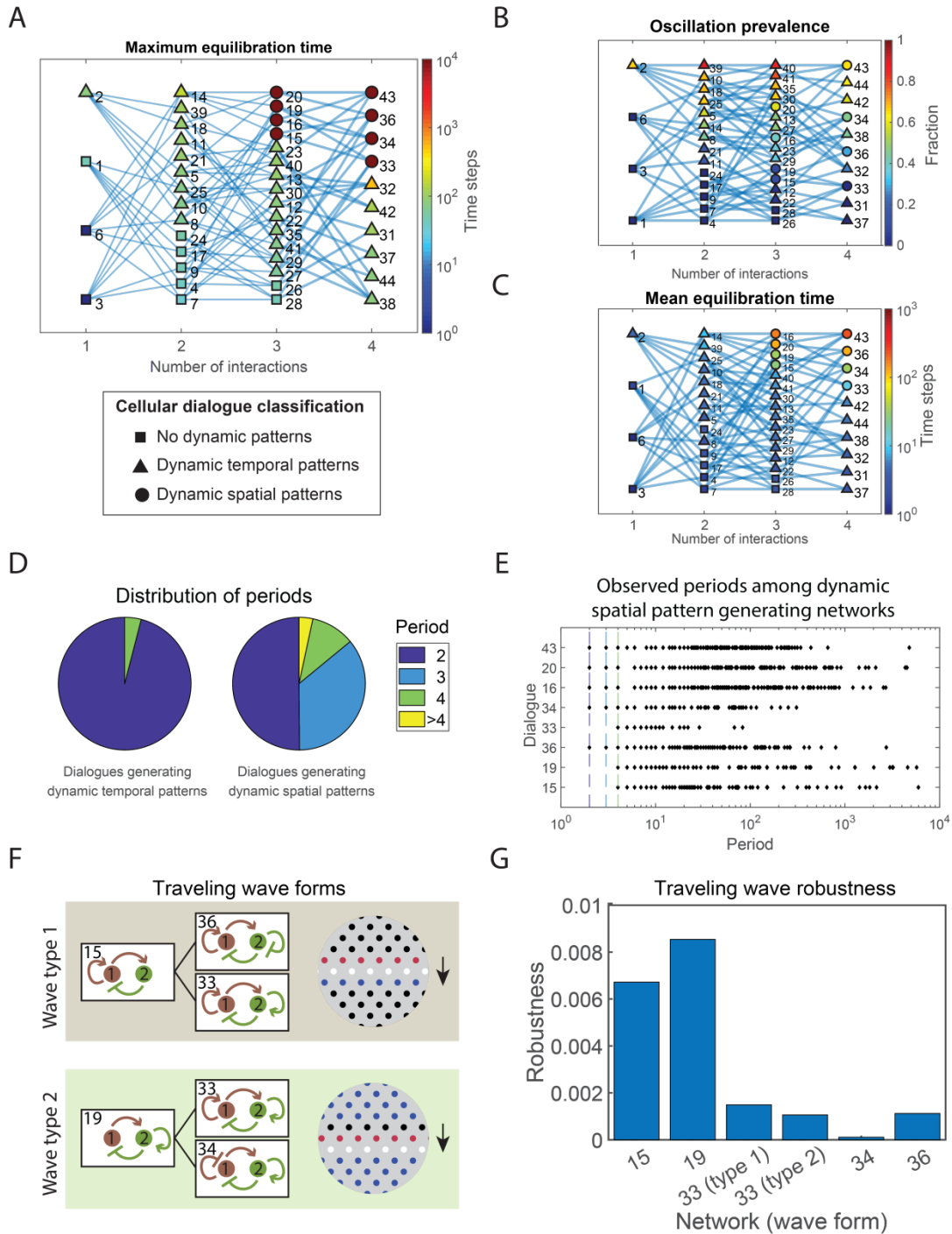


**Figure S13. How an OR-logic gate, instead of an AND-logic gate, affects the self-organization of static and dynamic patterns.**

*(Related to Figure 6)*

Results here can be compared with Figures 3B-E. Parameter sets are independently generated from Latin hypercube sampling, with  $10^4$  different parameter sets per cellular dialogue (see STAR Methods). **(A)** By measuring the "equilibration time" - time taken for a simulation to terminate due

to either forming a static configuration or a dynamic pattern - for many simulations that all used the same cellular dialogue, we obtained the largest possible (maximum) equilibration time. To ensure that we do not let a simulation run forever, we arbitrarily forced simulations to terminate after  $t_{\max} = 10^4$  timesteps if it has not already terminated by itself. **(B)** Fraction of simulations that exhibit a periodic pattern (i.e., a dynamic pattern that repeats itself after a fixed number of timesteps which is larger than one). **(C)** Averaging the equilibration times of all simulations for each cellular dialogue. **(D)** Distribution of periods for periodic patterns. Results shown for cellular dialogues that generate dynamic temporal patterns (Figure 3C) and cellular dialogues that also generate dynamic spatial patterns (Figure 3D). **(E)** Distribution of periods for periodic patterns for cellular dialogues that generate dynamic spatial patterns (Figure 3D). Each diamond represents a period that we observed in at least one simulation. **(F)** Wave configurations observed with the OR-logic (compare with the AND-logic shown in Figure 4D). **(G)** Robustness of wave propagation for all six instances of waves shown in (F), defined as the Q-value obtained from simulations (see Figure S6 for comparison with the AND-logic).

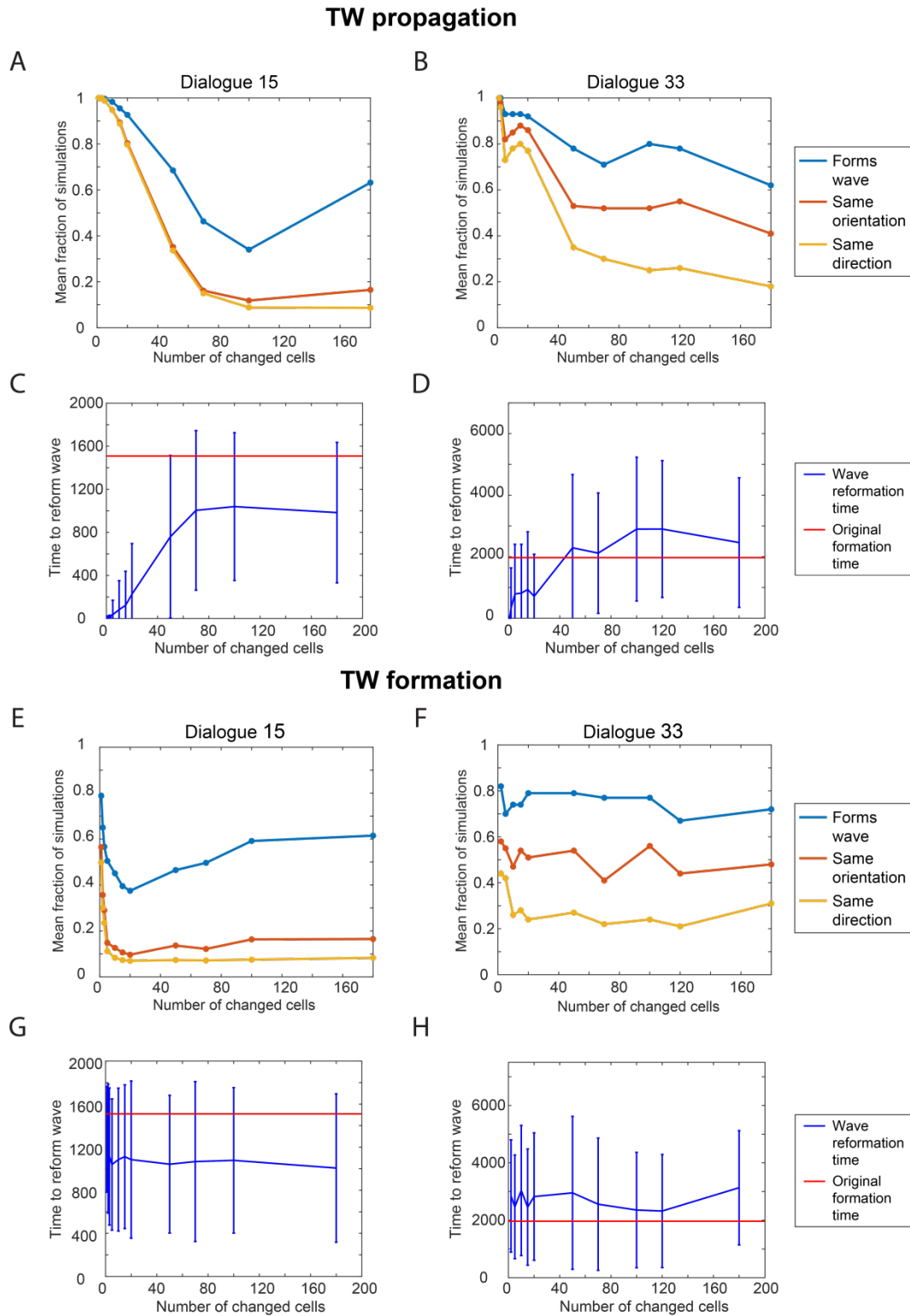


**Figure S14. Stability of waves under perturbations (see Supplemental Analysis Section S4.5).**

*(Related to Figure 6)*

We perturbed the initial spatial-configuration by randomly changing the gene expression of a fixed number of cells to see whether a wave could still form (in the case of starting with a disordered spatial configuration) or reform (in the case of already starting with a wave). Simulations were for cellular dialogue 15 (A, C, E, G) and cellular dialogue 33 (B, D, F, H). **(A-D)** Simulations start with a travelling wave, **(E-H)** Simulations start with a random state, which may eventually form a wave. In (A-B, E-F), we report the fraction of simulations in which a travelling wave (re)formed after the perturbation. We also compared whether the orientation and direction of the wave were preserved after the perturbation. In (C-D, G-H), we report the time taken to reform a TW after being perturbed, compared to the time that the simulation would have taken to form a TW without the perturbation. Error bars show standard deviations.